AT&T Technical Journal
Vol. 64, No. 10, December 1985
Printed in U.S.A.

Performance Signatures for Dual-Polarized Transmission of M-QAM Signals Over Fading Multipath Channels

By M. KAVEHRAD and C. A. SILLER, JR.*

(Manuscript received August 6, 1985)

Performance signatures for dual-polarized transmission of M-state quadrature amplitude-modulated signals over dispersive multipath digital radio channels are theoretically derived in this work. We report on two major findings. Firstly, we show that for the assumed propagation model, a cross-coupled interferer exhibits noiselike behavior and impacts on digital radio outage time in direct relation to its power level. Secondly, our theoretical finding is based on a new application of performance signature curves for two cross-coupled multipath channels. This treatment permits the prediction of multipath-induced digital radio outage for specified ratios of power in the copolarized and cross-coupled signals. Theoretical findings are qualitatively supported by measured performance signatures obtained from a laboratory simulation of the model.

I. INTRODUCTION

The last decade has witnessed a surge of interest in terrestrial digital radio transmission, with the newer high-capacity systems relying almost exclusively on single-polarization microwave transmission of M-state Quadrature Amplitude-Modulation (M-QAM) signals. In these digital radio systems, the performance degradation associated with multipath propagation has been of paramount importance and

*Authors are employees of AT&T Bell Laboratories.

the subject of considerable prior investigations. For single-polarization systems, the effects of multipath are well understood;[1,2] suitable countermeasures—particularly adaptive equalization—have been studied;[2-4] and these countermeasures are now widely deployed in a variety of digital radio systems.[5,6]

When compared with single-polarization systems, dual-polarized operation obviously engenders economic and efficient spectrum-utilization advantages. Unlike single-polarization transmission, however, an understanding of the effects of multipath propagation on this latter mode of operation is still in its infancy. For single-polarization operation, countermeasures to frequency-selective fading mitigate intersymbol interference (ISI) in the presence of Gaussian noise; the transmission of orthogonally polarized signals over the same bandlimited facility is similarly vulnerable to the effects of ISI and noise, but now Cross-Polarization Interference (CPI), normally suppressed by the polarization selectivity of the receiving antenna, is also present. Consequently, an optimal receiver must recover the transmitted signal in the presence of ISI, CPI, and noise.

Kavehrad[7] has previously studied dual-polarized M-QAM transmission over *nondispersive* media. He concluded that satisfactory transmission is not feasible without some form of cross-polarization interference cancellation. Furthermore, the work showed that in an optimal detection process, the total noise and CPI power must be adaptively minimized. In this paper we extended the scope of the previous work by considering dual-polarized transmission of M-QAM signals over *dispersive* fading channels like those experienced in line-of-sight applications.

The dual-polarized channel is modeled using Rummler-like[8] multipath transfer functions to describe both the copolarized and cross-coupled paths. The transfer functions emulate snapshots of independent multipath fading events on the copolarized and cross-coupled paths, which, in the presence of noise, limit the achievable error rate at the receiver. Our results are predicted on the major assumption that the two simultaneous fading events are statistically independent. Performance "signatures," defined by a locus of fade notch depths and frequency positions corresponding to a 10^{-3} error rate,[9] are used as a system performance measure since they are conveniently related to digital radio outage.[10]

For the assumed propagation model, we find that the cross-coupled interfering signal exhibits a noiselike behavior. That is, the power loss associated with a cross-coupled signal subject to flat or dispersive fading brings about an actual reduction in system outage time. Apparently, the deleterious effect of ISI contributed by dispersive fading of the cross-polarized interference is more than offset by the power loss

of the same associated with the fading event, consequently improving net system outage. Furthermore, this finding is supported by laboratory measurements in which the fading of two independent 16-QAM signals is simulated.

The theoretical and experimental finding cited above is based on a novel application of the aforementioned system performance signature curves for the propagation model adopted in this work. In particular, it permits an immediate comparison of multipath-induced dual-polarized digital radio outage for specified ratios of power in the copolarized signal and cross-coupled interferer.

In the following section we begin by providing a complete model of the dually polarized communication channel, including the influence of frequency-selective fading. In Section III the computational methods and performance measurers are discussed. Numerical results and laboratory measurements that support our finding are presented in Section IV. Our conclusions are summarized in Section V.

II. ANALYTICAL MODEL

2.1 Channel description

The system model for dual-polarized operation is illustrated in Fig. 1. Two independent data sources (one for each of the dual-polarized channels) are assumed to generate complex-valued symbols at the baud rate, $1/T_s$, where T_s is a symbol period. We denote these complex

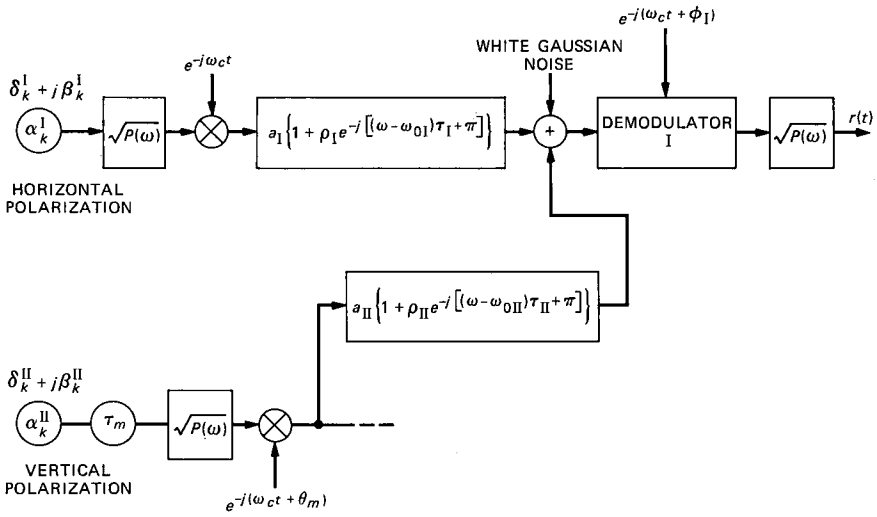

Fig. 1—Channel model for dual-polarized radio system.

symbols as

$$\alpha_k^i = \delta_k^i + j\beta_k^i \quad i = \text{I, II} \tag{1}$$

at consecutive instants kT_s, $k = 1, 2, 3 \cdots$. The index i denotes symbol sets transmitted on the main ($i = \text{I}$) and cross-coupled ($i = \text{II}$) channels. The real and imaginary parts $\{\delta_k^i, \beta_k^i\}$ take on discrete levels $\pm\Omega, \pm 3\Omega, \cdots, \pm(L-1)\Omega$ with equal probability. Parameter $L = \sqrt{M}$ is selected in accord with the number of states in the M-ary signal; the symbols δ and β are independent and identically distributed; and Ω is a measure of signal-point distance from the nearest decision boundary in signal space.

We assume each of the Pulse-Amplitude-Modulated (PAM) signals has a raised-cosine (Nyquist) spectral shaping with a roll-off factor Γ. The corresponding time-domain impulse shape is therefore[11]

$$p(t) = \frac{\sin(\pi t/T_s)}{\pi t/T_s} \cdot \frac{\cos(\Gamma \pi t/T_s)}{1 - (2\Gamma t/T_s)^2}, \tag{2}$$

and the frequency-domain transfer function is designated $P(\omega)$. On each of the orthogonally polarized channels, the shaped signals are modulated by quadrature carrier signals of frequency f_c. Furthermore, the two independent carrier local oscillators for $i = \text{I}$ and $i = \text{II}$ at the transmitter are out of phase by θ_m, where this phase difference is a uniformly distributed random variable over the range $0 \le \theta_m \le 2\pi$. The complex baseband symbol sequences are assumed misaligned by τ_m, where τ_m is also a uniformly distributed random variable over the range $0 \le \tau_m \le T_s$.

As previously stated, we follow Rummler's prescription for modeling multipath fading. The model is applied to both the copolarized ($i = \text{I}$) and the cross-coupled ($i = \text{II}$) signal paths and assumes the presence of a single inband notch in each of the main and cross-coupled path transfer functions. This latter assumption of notched fading in the cross-coupled signal band and notched fading in the main polarized signal band agrees with recent measurements that indicate the possibility of a shallow fade notch in the interfering cross-coupled path.[12]

For our analysis we use "static" fading models to emulate "snapshots" of multipath fading events.[13] The passband transfer function for the two-ray propagation model can be expressed as

$$F(\omega) = a\{1 + \rho e^{-j[(\omega-\omega_0)\tau+\pi]}\}, \tag{3}$$

where a represents the flat fade level and all other parameters are related to dispersive fading as follows: the fade notch depth is $-20 \log |1 - \rho|$, where ρ is the relative amplitude of the secondary ray;* the

* For minimum phase fades with $\rho < 1$.

relative delay between rays is τ and ω_0 is the fade notch frequency. For a fade notch centered in the passband,

$$\tau = \frac{2n\pi}{\omega_c - \omega_0}, \tag{4}$$

where ω_c is the radian carrier frequency.

In the absence of a cross-coupled interfering signal, the main polarization baseband waveform after demodulation at the receiver, as shown in Fig. 1, can be expressed as

$$x_{\mathrm{I}}(t) = \sum_k \alpha_k^{\mathrm{I}} h_{\mathrm{I}}(t - kT_s) e^{-j\phi_{\mathrm{I}}} + n_{\mathrm{I}}(t), \tag{5}$$

where

$$h_{\mathrm{I}}(t) = a_{\mathrm{I}}\{p(t) + \rho_{\mathrm{I}} p(t - \tau_{\mathrm{I}}) e^{-j[(\omega_c - \omega_{0\mathrm{I}})\tau_{\mathrm{I}} + \pi]}\} \tag{6}$$

is the low-pass equivalent of the channel impulse response. The index I in eqs. (5) and (6) explicitly denotes reference to the main polarization channel; $n_{\mathrm{I}}(t)$ is filtered Gaussian noise with variance $\sigma_{n_{\mathrm{I}}}^2$; and ϕ_{I} represents the relative phase difference between the modulator and demodulator oscillators. In terms of a specific sampling epoch, t_0, distortion in the overall channel impulse response is minimized by an optimum relative carrier phase[3]

$$\phi_{\mathrm{I,opt}}(t_0) = -\operatorname{Arc\,tg} \frac{\rho_{\mathrm{I}} p(t_0 - \tau_{\mathrm{I}}) \sin[(\omega_c - \omega_{0\mathrm{I}})\tau_{\mathrm{I}} + \pi]}{p(t_0) + \rho_{\mathrm{I}} p(t_0 - \tau_{\mathrm{I}}) \cos[(\omega_c - \omega_{0\mathrm{I}})\tau_{\mathrm{I}} + \pi]}. \tag{7}$$

Extending the above discussion to dual-polarized operation, we give the received baseband signal in the main polarization channel as

$$r_{\mathrm{I}}(t) = \sum_k \alpha_k^{\mathrm{I}} h_{\mathrm{I}}(t - kT_s) e^{-j\phi_{\mathrm{I}}} + \sum_k \alpha_k^{\mathrm{II}} h_{\mathrm{II}}(t - kT_s - \tau_m) e^{-j(\phi_{\mathrm{I}} + \theta_m)} + n_{\mathrm{I}}(t), \tag{8}$$

where h_{I} and h_{II} represent the low-pass equivalents of the main and cross-coupled paths impulse responses, respectively. As long as the main signal [the first term in eq. (8)] is much stronger than the cross-coupled interferer, the carrier phase tracked by the demodulator of the main polarization receiver is the relative phase difference between local oscillators of the main polarization modulator and demodulator, $\phi_{\mathrm{I,opt}}(t_0)$. In its expanded form, eq. (8), representing the demodulated composite signal at the main polarization receiver, can be expressed as

$$
\begin{aligned}
r_{\mathrm{I}}(t) = & \sum_k (\delta_k^{\mathrm{I}} + j\beta_k^{\mathrm{I}}) \\
& \times \{a_{\mathrm{I}} p(t - kT_s) + a_{\mathrm{I}}\rho_{\mathrm{I}} p(t - kT_s - \tau_{\mathrm{I}}) e^{-j[(\omega_c - \omega_{0\mathrm{I}})\tau_{\mathrm{I}} + \pi]} e^{-j\phi_{\mathrm{I}}}\} \\
& + \sum_k (\delta_k^{\mathrm{II}} + j\beta_k^{\mathrm{II}}) \\
& \times \{a_{\mathrm{II}} p(t - kT_s - \tau_m) + a_{\mathrm{II}}\rho_{\mathrm{II}} p(t - kT_s - \tau_{\mathrm{II}} - \tau_m) \\
& \cdot e^{-j[(\omega_c - \omega_{0\mathrm{II}})\tau_{\mathrm{II}} + \pi]} e^{-j(\phi_{\mathrm{I}} + \theta_m)} + n_{\mathrm{I}}(t). \qquad (9)
\end{aligned}
$$

Notice that the parameters of the two independent fading events can be varied independently.

To establish the relationship of eq. (9) to probability of error, and ultimately derive the performance signature (M curve)[9] that describes outage performance for a 10^{-3} symbol error rate, we can focus on the in-phase or quadrature rail signal on the received main polarization. Because the signal constellations are symmetrical, the associated probability of error for each of those two rails is identical and the *total* symbol error rate can be determined. From eq. (9) the in-phase component of the received signal is clearly $\mathrm{Re}[r_{\mathrm{I}}(t)] \equiv r_{i,\mathrm{I}}(t)$:

$$
\begin{aligned}
r_{i,\mathrm{I}}(t) = & a_{\mathrm{I}}\delta_0^{\mathrm{I}}\{\cos(\phi_{\mathrm{I}})p(t) + \rho_{\mathrm{I}}\cos[(\omega_c - \omega_{0\mathrm{I}})\tau_{\mathrm{I}} + \pi + \phi_{\mathrm{I}}]p(t - \tau_{\mathrm{I}})\} \\
& + a_{\mathrm{I}} \sum_{k\neq 0} \delta_k^{\mathrm{I}}\{\cos(\phi_{\mathrm{I}})p(t - kT_s) \\
& + \rho_{\mathrm{I}}\cos[(\omega_c - \omega_{0\mathrm{I}})\tau_{\mathrm{I}} + \pi + \phi_{\mathrm{I}}]p(t - kT_s - \tau_{\mathrm{I}})\} \\
& + a_{\mathrm{I}} \sum_k \beta_k^{\mathrm{I}}\{\sin(\phi_{\mathrm{I}})p(t - kT_s) \\
& + \rho_{\mathrm{I}}\sin[(\omega_c - \omega_{0\mathrm{I}})\tau_{\mathrm{I}} + \pi + \phi_{\mathrm{I}}]p(t - kT_s - \tau_{\mathrm{I}})\} \\
& + a_{\mathrm{II}} \sum_k \delta_k^{\mathrm{II}}\{\cos(\phi_{\mathrm{I}} + \theta_m)p(t - kT_s - \tau_m) \\
& + \rho_{\mathrm{II}}\cos[(\omega_c - \omega_{0\mathrm{II}})\tau_{\mathrm{II}} + \pi + \phi_{\mathrm{I}} + \theta_m] \\
& \cdot p(t - kT_s - \tau_{\mathrm{II}} - \tau_m)\} \\
& + a_{\mathrm{II}} \sum_k \beta_k^{\mathrm{II}}\{\sin(\phi_{\mathrm{I}} + \theta_m)p(t - kT_s - \tau_m) \\
& + \rho_{\mathrm{II}}\sin[(\omega_c - \omega_{0\mathrm{II}})\tau_{\mathrm{II}} + \pi + \phi_{\mathrm{I}} + \theta_m] \\
& \cdot p(t - kT_s - \tau_{\mathrm{II}} - \tau_m)\} + \mathrm{Re}[n_{\mathrm{I}}(t)], \qquad (10)
\end{aligned}
$$

and we denote the real part of the thermal noise by $n_{i,\mathrm{I}}(t)$. The preceding remarks are germane to modeling the channel. In the following subsection we relate the received in-phase baseband signal,

given by eq. (10), to the associated probability-of-error performance of the dual-polarized QAM radio system.

2.2 *Probability-of-error considerations*

Denoting the coefficient of the desired detected in-phase state as Z_0, we have

$$Z_0 = a_I\{\cos(\phi_I)p(t_0) + \rho_I\cos[(\omega_c - \omega_{0I})\tau_I + \pi + \phi_I]p(t_0 - \tau_I)\}, \quad (11)$$

where t_0, the sampling time, is optimized by mimizing the distortion contributed by the second and third terms in eq. (10). The set of slicing levels at the in-phase detector of the main polarization receiver can be set to

$$\{-(L-2)\Omega Z_0, \cdots, -2\Omega Z_0, 0, 2\Omega Z_0, \cdots, (L-2)\Omega Z_0\},$$

and, with no loss of generality, we set $\Omega = 1$.

Designating the sum of ISI contributed by dispersion in the main polarization and cross-coupled interference at the optimum sampling time t_0 by $\chi(\delta_k^I, \delta_k^{II}, \beta_k^I, \beta_k^{II})$, eq. (10) reduces to

$$r_{i,I}(t_0) = \delta_0^I Z_0 + \chi(\delta_k^I, \delta_k^{II}, \beta_k^I, \beta_k^{II}) + n_{i,I}(t_0). \quad (12)$$

Considering the automatic gain control operation at the receiver, the associated probability of error is then

$$P_{e,I_i} = 2\left[\frac{L-1}{L}\right]P_r\{(n_{i,I} + \chi) > Z_0\}. \quad (13)$$

Also, note that the noise variance $\sigma_{n_{i,I}}^2$ is equal to the total filtered noise variance, subsequently denoted by σ_n^2. Additionally,

$$P_r\{(\chi + n_{i,I}) > Z_0\} = E_{\chi,n_I}\{P_r[n_{i,I} > (Z_0 - \chi) \mid \chi = x]\}, \quad (14)$$

where $E\{\cdot\}$ denotes statistical averaging and x is the conditioned value of random variable χ. First, taking the average over the Gaussian noise, we obtain

$$P_r\{(\chi + n_{i,I}) > Z_0\} = \frac{1}{2}E_\chi\left\{\text{erfc}\left(\frac{Z_0 - x}{\sqrt{2}\ \sigma_n}\right)\right\}, \quad (15)$$

where the complementary error function, erfc(ϵ), is defined by

$$\text{erfc}(\epsilon) = \frac{2}{\sqrt{\pi}}\int_\epsilon^\infty e^{-\eta^2}d\eta\,. \quad (16)$$

By symmetry of the constellation, the total symbol error rate can therefore be expressed as

$$P_e \approx 2P_{e,I_i} = 2\,\frac{L-1}{L}\int_x \text{erfc}\left(\frac{Z_0 - x}{\sqrt{2}\ \sigma_n}\right)dF(x), \quad (17)$$

where $F(x)$ is the cumulative distribution function for the random variable χ.

The integration in eq. (17) can be evaluated using Gauss Quadrature Rules (GQR).[14] Equation (17) is thus expressed as

$$P_e \approx 2\frac{L-1}{L}\sum_{j=1}^{N} w_j \operatorname{erfc}\left[\frac{Z_0-\xi_j}{\sqrt{2}\,\sigma_n}\right]. \tag{18}$$

In this equation, N is the number of terms in the finite series, and w_j and ξ_j are weights and nodes in the GQR approximation. At this point, P_e in eq. (18) is calculated from the $N_0 = 2N + 1$ moments of χ. Because χ is functionally dependent upon the independent transmitted symbol states, we have adopted Prabhu's algorithm[15] to determine the moments. Note that the moments obtained in this manner are conditioned on the values of the two random variables τ_m and θ_m. Hence, the resulting moments must be averaged over $\{\tau_m, \theta_m\}$ before they can be used in the GQR method.

To derive the probability of symbol error as a function of signal-to-noise ratio (s/n), we define

$$\gamma = \frac{L^2-1}{3}\frac{\Omega^2}{\sigma_n^2} \tag{19}$$

as the s/n. Using this relationship, we rewrite eq. (18) as

$$P_e = 2\frac{L-1}{L}\sum_{j=1}^{N} w_j \operatorname{erfc}\left[(Z_0-\xi_j)\sqrt{3\gamma/2(L^2-1)}\right], \tag{20}$$

where we have normalized Ω to one. In the next section we expand further on the computational aspects of the GQR method.

As previously stated, the relationships above are all dependent upon the timing phase. This parameter can be selected a posteriori to minimize P_e, thus making probability-of-error computations a formidable, numerically intensive task. In this work we choose a priori sampling epoch by minimizing the peak distortion of the received signal prior to equalization. The timing phase is thus dependent on both the in-phase and quadrature rails of the main polarization M-QAM signal.

2.3 Signal-to-interference ratio

In addition to performance signature, we have also evaluated at select points along the M curve a corresponding signal-to-interference ratio (SIR). This ratio is defined as the relative power in the main polarization to that of the cross-coupled interfering signal. Using parameters previously defined, this ratio is simply

SIR

$$= \frac{a_{\mathrm{I}}^2 \int_0^{(1+\Gamma)\pi/T_s} |P(\omega)|^2\{1 + \rho_{\mathrm{I}}^2 - 2\rho_{\mathrm{I}}\cos[(\omega - \omega_{0\mathrm{I}})\tau_{\mathrm{I}}]\}d\omega}{a_{\mathrm{II}}^2 \int_0^{(1+\Gamma)\pi/T_s} |P(\omega)|^2\{1 + \rho_{\mathrm{II}}^2 - 2\rho_{\mathrm{II}}\cos[(\omega - \omega_{0\mathrm{II}})\tau_{\mathrm{II}}]\}d\omega}, \quad (21)$$

by which we can observe changes in the average SIR.

III. NUMERICAL ANALYSIS

An examination of Section II demonstrates that the theoretical analysis of M-QAM signal transmission over dual-polarized facilities in the presence of multipath fading is a computationally exhaustive activity. In this section we provide a brief overview of numerical issues related to our investigation.

3.1 Impulse response description

It is easily seen [see eq. (9) or (10)] that the dispersive nature of the multipath channel is completely described by the superposition of four impulse responses, each independently weighted by an appropriate transmitted symbol state. These impulse responses for the kth transmitted symbol are

$$u_{i,\mathrm{I}}(t) = a_{\mathrm{I}}\{p(t - kT_s)\cos(\phi_{\mathrm{I}}) + \rho_{\mathrm{I}}p(t - kT_s - \tau_{\mathrm{I}})\cos[(\omega_c - \omega_{0\mathrm{I}})\tau_{\mathrm{I}} + \pi + \phi_{\mathrm{I}}]\}, \quad (22a)$$

$$u_{q,\mathrm{I}}(t) = a_{\mathrm{I}}\{p(t - kT_s)\sin(\phi_{\mathrm{I}}) + \rho_{\mathrm{I}}p(t - kT_s - \tau_{\mathrm{I}})\sin[(\omega_c - \omega_{0\mathrm{I}})\tau_{\mathrm{I}} + \pi + \phi_{\mathrm{I}}]\}, \quad (22b)$$

$$u_{i,\mathrm{II}}(t) = a_{\mathrm{II}}\{p(t - kT_s - \tau_m)\cos(\phi_{\mathrm{I}} + \theta_m) + \rho_{\mathrm{II}}p(t - kT_s - \tau_{\mathrm{II}} - \tau_m)\cos[(\omega_c - \omega_{0\mathrm{II}})\tau_{\mathrm{II}} + \pi + \phi_{\mathrm{I}} + \theta_m]\}, \quad (22c)$$

and

$$u_{q,\mathrm{II}}(t) = a_{\mathrm{II}}\{p(t - kT_s - \tau_m)\sin(\phi_{\mathrm{I}} + \theta_m) + \rho_{\mathrm{II}}p(t - kT_s - \tau_{\mathrm{II}} - \tau_m)\sin[(\omega_c - \omega_{0\mathrm{II}})\tau_{\mathrm{II}} + \pi + \phi_{\mathrm{I}} + \theta_m]\}, \quad (22d)$$

where the variables have been previously defined. In the in-phase rail of the main polarization receiver, eqs. (22a) and (22b) describe the distorted in-phase and quadrature-coupled signals from the main polarization transmitter, respectively, and eqs. (22c) and (22d) describe the corresponding signals from the cross-coupled interferer signal. The optimum timing phase, $t_{0,\mathrm{opt}}$, is selected by minimizing the peak distortion embedded in eqs. (22a) and (22b). That peak distortion is

$$D_p(t_0) = \frac{1}{u_{i,\mathrm{I}}(t_0,\ k=0)} \left\{ \sum_{\substack{k=-\infty \\ k\neq 0}}^{\infty} |u_{i,\mathrm{I}}(t_0)| + \sum_{k=-\infty}^{\infty} |u_{q,\mathrm{I}}(t_0)| \right\}. \quad (23)$$

Distortion contributed by $u_{i,\mathrm{II}}$ and $u_{q,\mathrm{II}}$ is specifically excluded from eq. (23) since the complex data sources I and II are not coherent; these latter signals appear noiselike to the timing recovery circuit in the main polarization receiver.

From a computational standpoint, the operations described above are carried out by first computing $\phi_{\mathrm{I,opt}}(t_0)$ and $D_p(t_0)$ for all t_0 in the range $[-T_s, T_s]$, and then selecting the single sampling epoch, $t_{0,\mathrm{opt}}$, that minimizes D_p. With $t_{0,\mathrm{opt}}$ identified, the symbol-period spaced samples of $u_{i,\mathrm{I}}$, $u_{q,\mathrm{I}}$, $u_{i,\mathrm{II}}$, and $u_{q,\mathrm{II}}$ are used for the subsequent probability-of-error computations. An a priori selection of $t_{0,\mathrm{opt}}$ obviously expedites the computer time necessary to perform the probability-of-error computations. The use of a timing phase that minimizes peak distortion is one such choice. Another choice could be minimization of mean-square eye closure. This can be shown to be equivalent to an IF timing recovery.

For *illustrative* purposes, we present plots of $u_{i,\mathrm{I}}$, $u_{q,\mathrm{I}}$, $u_{i,\mathrm{II}}$, and $u_{q,\mathrm{II}}$ in Fig. 2 for $\rho_{\mathrm{I}} = 0.80$, $\rho_{\mathrm{II}} = 0.75$, $a_{\mathrm{I}} = 1.0$, $a_{\mathrm{II}} = 0.5$, $f_{0\mathrm{I}} = 1.63$ MHz, $f_{0\mathrm{II}} = 0$ MHz, $\Gamma = 0.45$, $\tau_m = 0$, $\theta_m = 0$, and $T_s = 1/(15$ Mbaud). For this illustration example, $t_{0,\mathrm{opt}} = -0.4\,T_s$ and $\phi_{\mathrm{I,opt}} = 5.13°$. In particular, note that this carrier phase nulls the $u_{q,\mathrm{I}}$ response at $t = t_{0,\mathrm{opt}}$, as it should. However, even though the cross-coupled interferer corresponds

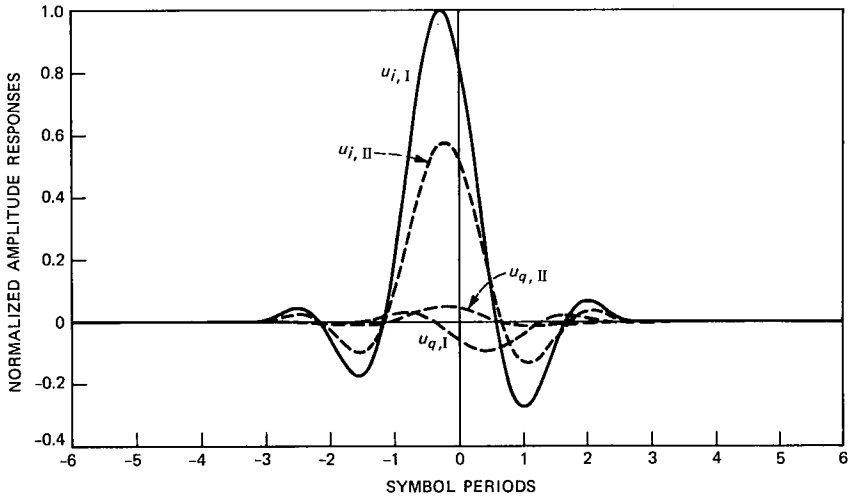

Fig. 2—Dispersive effects on impulse responses of a dual-polarized digital radio system.

to a notch-centered fade and $\theta_m = 0$, $u_{q,\mathrm{II}} \neq 0$ since the carrier phase optimization is independent of channel II.

3.2 Signal-to-interference evaluation

The signal-power-to-interference-power ratio was evaluated from eq. (21). The presence of $|P(\omega)|^2$ in this expression derives from the fact that at the receiver, the main and interference signals have $P(\omega)$ spectral shaping and thus a $|P(\omega)|^2$ spectral power density. The $a_i^2\{1 + \rho_i^2 - 2\rho_i \cos[(\omega - \omega_{0i})\tau_i]\}$, $i = \mathrm{I}, \mathrm{II}$, terms correspond to spectral power density associated with the dispersive fade and the undistorted signal power. The integral is conveniently evaluated using Romberg-quadrature methods.

3.3 Probability-of-error computations

As explained in Section 3.1, the in-phase component of the received signal on the main polarization has basically four parts. The desired symbol to be detected is the $k = 0$ term of $u_{i,\mathrm{I}}(t)$ in eq. (22a). Each of the four aforementioned terms consists of a sum of weighted, independent, identically distributed random variables that together were designated as $\chi(\delta_k^{\mathrm{I}}, \beta_k^{\mathrm{I}}, \delta_k^{\mathrm{II}}, \beta_k^{\mathrm{II}})$ and discussed in Section 3.2. Since the random variable χ is in the form of a sum of sums of independent random variables, it can be considered a long sum of weighted, independent random variables. Thus, to determine a finite number of moments of χ, Prabhu's[15] recursive algorithm can be used: If

$$\Delta_k = \sum_{i=1}^{k} \nu_i, \tag{24}$$

then

$$\begin{aligned} \psi_{N_0}(k) &= E\{[\Delta_{k-1} + \nu_k]^{N_0}\} \\ &= \sum_{t=0}^{N_0} \binom{N_0}{t} \psi_t(k-1) E\{\nu_k^{(N_0 - t)}\}. \end{aligned} \tag{25}$$

Based on this recursive formula, a computer program was written to calculate N_0 moments of the random variable χ.

Since all zero-mean random variables involved in the sum are evenly distributed, the odd moments of the sum become zero. In all our computations, $N_0 = 31$ moments were found to be adequate for the probability-of-error calculations.

Following the computation of conditional moments of χ by averaging over uniformly distributed variables τ_m and θ_m, the absolute moments of χ were found and subsequently used with the GQR method for computing the error probabilities. (For a brief summary of GQRs see Appendix C of Ref. 17.) For additional detail, interested readers are

referred to Ref. 14. Observe that by averaging over $\alpha_k^i (i = \text{I, II})$, τ_m, and θ_m when computing the N_0 moments ψ_{N_0}, a great deal of computation time is saved because these calculations are made *once* for all s/n values.

IV. NUMERICAL AND EXPERIMENTAL RESULTS

In this section we present theoretical and measured performance signature curves for dual-polarized digital radio. It is well known that signature curves provide a locus of fade notch depths (in decibels) and relative fade notch positions (Hz) for a 10^{-3} probability of error. However, unlike their more customary presentation, we must also include parameters that define the character of the interfering cross-coupled multipath channel.

4.1 Theoretical performance signatures

As a reference, we have computed the signature of a singularly polarized 16-QAM system, that is, $a_{\text{II}} = 0$. The data are presented in Fig. 3 and labeled "1." Along this contour we also designate the SIR (in decibels) computed using methods previously described. For the case of no cross-coupled interferer, the SIR is obviously infinite. For all other cases, the SIR value at each point on the signature curve is functionally dependent upon specific fading parameters for the main and cross-coupled signals. Moreover, we associate with each curve a triplet representing the dispersive fading status of the cross-coupled interferer. This triplet is

$$\left[20 \log \frac{a_{\text{II}}}{a_{\text{I}}} \text{ (in dB)}, -20 \log|1 - \rho_{\text{II}}| \text{ (in dB)}, \text{ and } \Delta f_{0\text{II}} \text{ (in MHz)}\right],$$

where Δf_{0i}, $i = \text{I, II}$, denotes fade notch positions relative to the carrier. For example, the triplet (−30, 5, 11) describes a cross-coupled signal with a flat power level 30 dB below that of the main polarization with a 5-dB inband fade notch located 11 MHz away from the carrier frequency. For the case of curve 1 in Fig. 3, the triplet is simply $(-\infty, \cdot, \cdot)$.

In addition to curve 1 in Fig. 3, we show three other cases corresponding to (−30, 10, 0), (−30, 5, 0), and (−30, 5, 11) and denoted 2, 3, and 4, respectively. A comparison of curves 2 and 3, with the same −30 dB flat power levels and 0-MHz notch offsets, reveals that the fade of curve 2, with a 10-dB inband notch, results in *less* outage time than the fade of curve 3, with 5-dB inband notch. Hence, the greater power loss associated with curve 2 leads to reduced outage, even though the intersymbol interference for curve 2 exceeds that of curve 3. Now

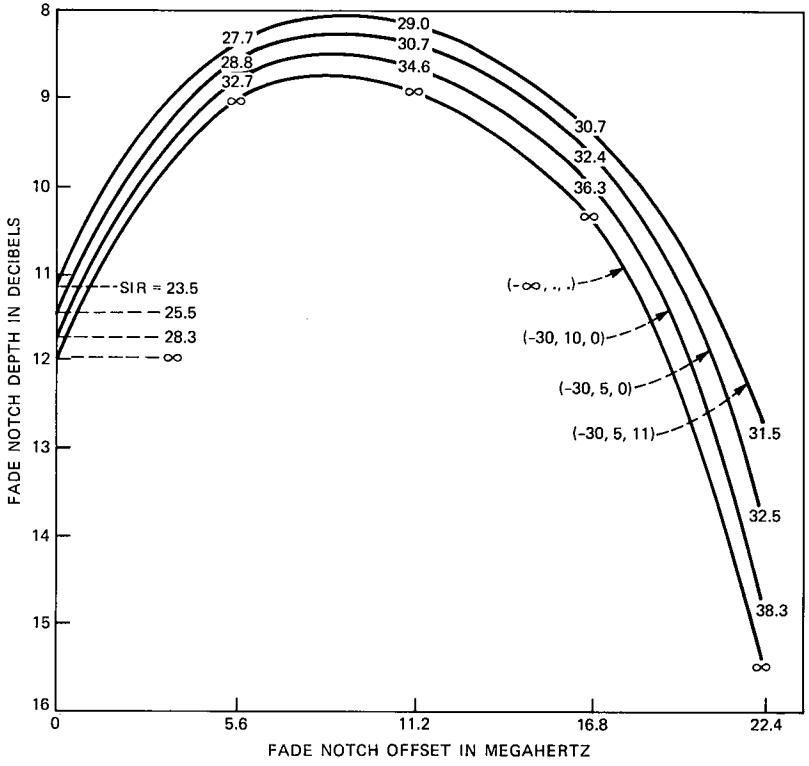

Fig. 3—Performance signature curves for dual-polarized 16-QAM radio; $\Gamma = 0.45$, $T_s = 1/(22.5$ Mbaud), $s/n = 60$ dB. Curves 1 through 4 show relationship of SIR to relative digital radio outage.

consider curves 3 and 4. This data corresponds to identical flat power levels and fade notch depths, with the notch position moving from 0 MHz (notch centered) to 11 MHz (near the band edge). The notch-centered fade apparently causes less outage than the notch offset fade. When we remember that the unfaded signal spectral energy at 0 MHz is much more than that near 11 MHz, it should be clear that the relationship of curves 3 and 4 is again that of diminished net signal power in the interferer that equates to a reduced outage.

SIR values are listed at certain points along curves 2, 3, and 4. It will be noted that moving toward higher notch offset values on each performance signature results in greater SIRs, specifically for the reason cited above. A fade positioned in a region of normally high spectral energy will pull out more power than the same fade in a region of reduced spectral energy. Moreover, at any main polarization notch frequency position, the SIR increases as the performance signature drops, because interference signal power, rather than intersymbol

interference, is the dominant factor for outage due to an independent interferer.

To further verify that interference power plays a major role in outage performance, Fig. 4 presents two relevant cases. In that figure we consider (−30, 0, 0) and (−25, 5, 0) dispersive fading of 16-QAM cross-coupled signals. In both cases the total interference power loss is approximately the same. The former case corresponds to a 30-dB flat fade of the interferer, while in the latter case the flat fade is 25 dB with a 5-dB shaped fade positioned in the center of the passband (a region of high spectral energy). Observe that the outage performance and SIR are virtually identical along the entire signature curves. We therefore conclude that whether fading of the cross-coupled signal is mildly dispersive (i.e., generating intersymbol interference) or flat, outage performance improvement is accompanied by interference power reduction provided the flat level of the cross-coupled signal is considerably below that of the main polarization signal (this is normally the case because of antenna/waveguide polarization isolation) and the dispersive fading of the cross-coupled signal is shallow.

To confirm that the aforementioned property holds at lower isolation levels as well, we have repeated the performance signature cal-

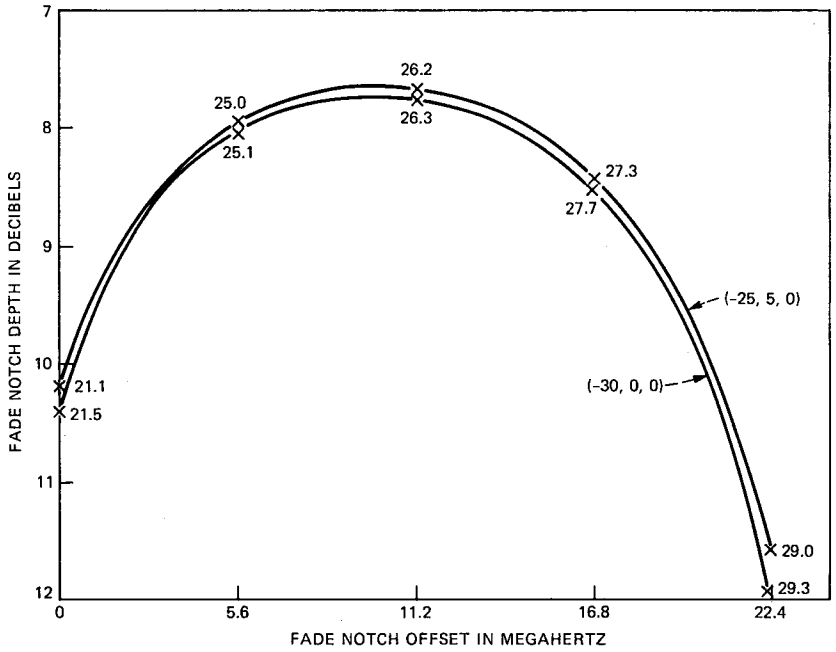

Fig. 4—Performance signature curves for dual-polarized 16-QAM radio; $\Gamma = 0.45$, $T_s = 1/(22.5 \text{ Mbaud})$, $s/n = 60$ dB. The total interference power loss is approximately the same, as is the relative digital radio outage.

culations for an interfering signal flat fade level of −20 dB. The results, presented in Fig. 5, confirm those in Figs. 3 and 4.

Up to now θ_m and τ_m were taken to be random variables. To gain further insight, we now impose $\theta_m = 0$ and $\tau_m = 0$ conditions on the interfering signal, thereby illustrating a case for which timing and carrier phase of the two signals are aligned. We have repeated computations for the case presented in Fig. 5. These computations are presented in Fig. 6. Observe that the same qualitative properties hold. In the case of a (−20, 0, 0) interfering signal, the synchronous system exhibits a lower outage time than the general system for the same interferer (see Fig. 5).

Data in Figs. 3 through 6 were all computed for a 60-dB s/n, 22.5-Mbaud symbol rate, $\Gamma = 0.45$ roll-off, 16-QAM dually polarized radio system. We have repeated these performance signature computations for a 66-dB s/n, 15-Mbaud, $\Gamma = 0.45$, 64-QAM dually polarized radio system. The resulting curves, shown in Fig. 7, are expectedly much wider than the 16-QAM case. However, the general phenomenon exhibited by the data of Figs. 3 through 6 remains appropriate to Fig. 7, as well.

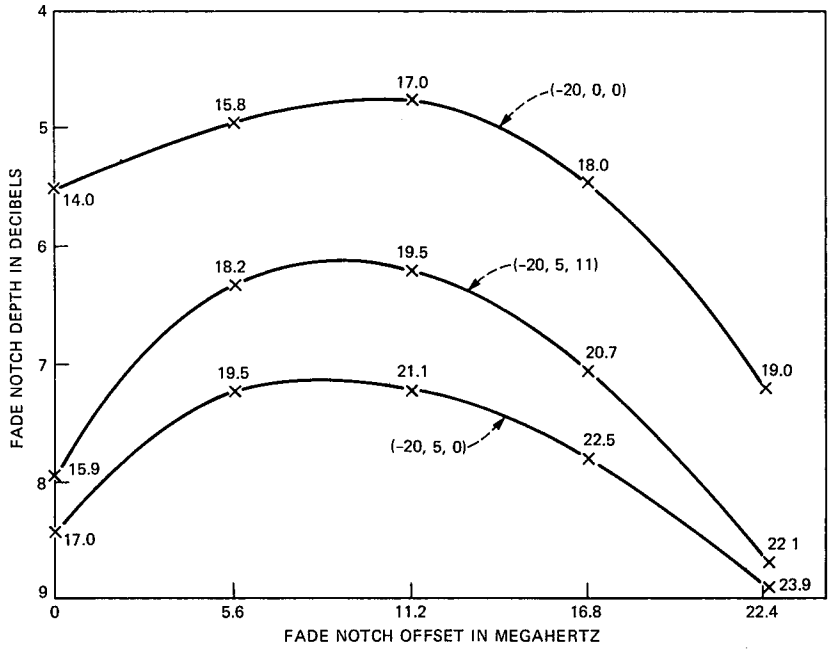

Fig. 5—Performance signature curves for dual-polarized 16-QAM radio; $\Gamma = 0.45$, $T_s = 1/(22.5 \text{ Mbaud})$, $s/n = 60$ dB. These cases correspond to lower isolation levels than those in Figs. 3 and 4.

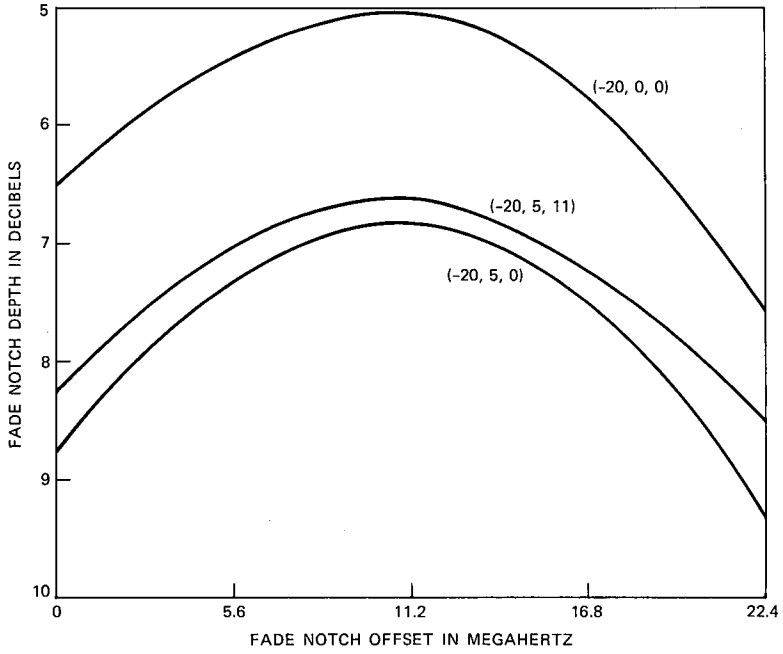

Fig. 6—Performance signature curves for dual-polarized 16-QAM radio; $\Gamma = 0.45$, $T_s = 1/(22.5 \text{ Mbaud})$, $s/n = 60$ dB, $\theta_m = 0$, and $\tau_m = 0$.

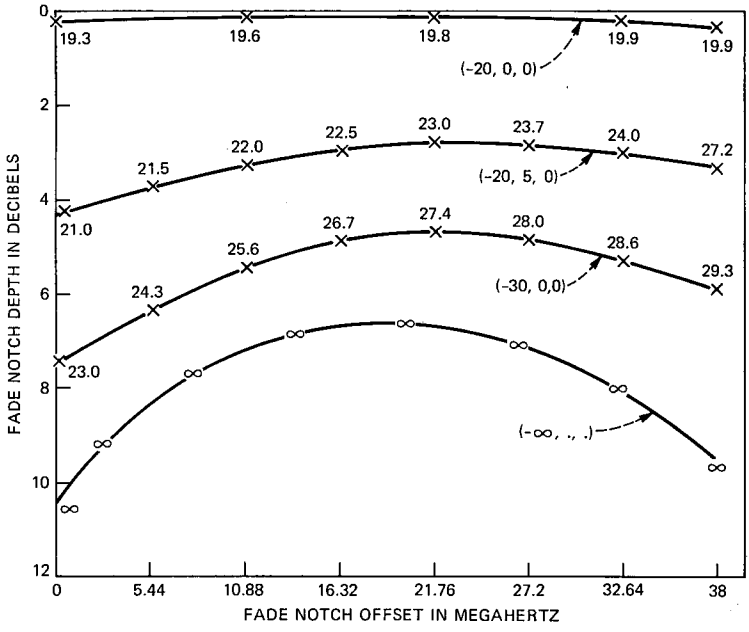

Fig. 7—Performance signature curves for dual-polarized 64-QAM radio; $\Gamma = 0.45$, $T_s = 1/(15 \text{ Mbaud})$, $s/n = 66$ dB.

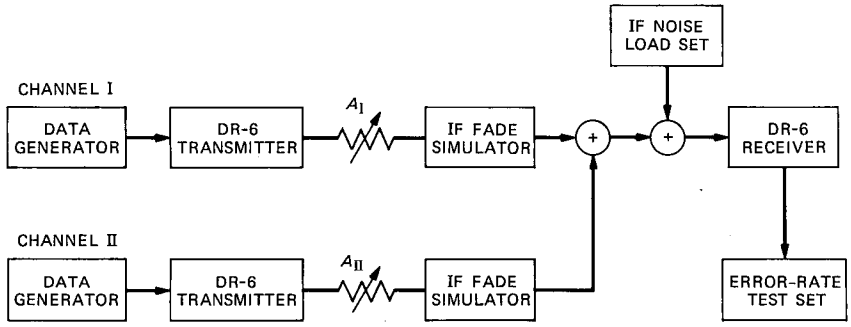

Fig. 8—Experimental facility for the measurement of dual-polarized digital radio performance signatures.

V. EXPERIMENT RESULTS

Using the experimental arrangements functionally illustrated in Fig. 8, we have confirmed the theoretical conclusions discussed in the previous section. As noted in the figure, two independent data sources provide inputs to DR-6* transmitters for channels I and II. The flat power levels of the two outputs are separately adjusted using attenuators A_I and A_{II}, and dispersive fading is provided by IF fade simulators. The channel I and II signals are added together with low-level noise (60-dB s/n) from an IF noise load set. The composite signal, simulating independent fading of a main polarization and a cross-coupled interferer, is then applied to a DR-6 receiver and error-rate test set.

Attenuators A_I and A_{II} were used to adjust the ratio a_{II}/a_I. Power was measured at the output of the IF fade simulators to establish the SIR and again at the input to the radio receiver to assure the demodulator had the appropriate signal level.

Error-rate measurements were made for a number of different fading events. The first set of measurements correspond to the triplets $(-\infty, 0, 0)$ and $(-25, 0, 0)$, the latter triplet representing a *flat*, nondispersive fade of the interferer. The performance signatures are presented in Fig. 9 and show the same trend as the theoretical data of Figs. 3 and 7. The quantitative differences are to be expected owing to equipment imperfections, such as nonideal Nyquist and bandpass filters, and imperfect carrier and timing recovery circuit operations. We next examined the influence of a dispersive fade characterized by $(-25, 5, 0)$. As expected, the performance signature improved, but not to the point of reaching the $(-\infty, 0, 0)$ case. This observation agrees with the data of Figs. 3, 5, and 7.

* DR-6 is a 16-QAM, 90-Mb/s, 22.5-Mbaud digital radio system.[16]

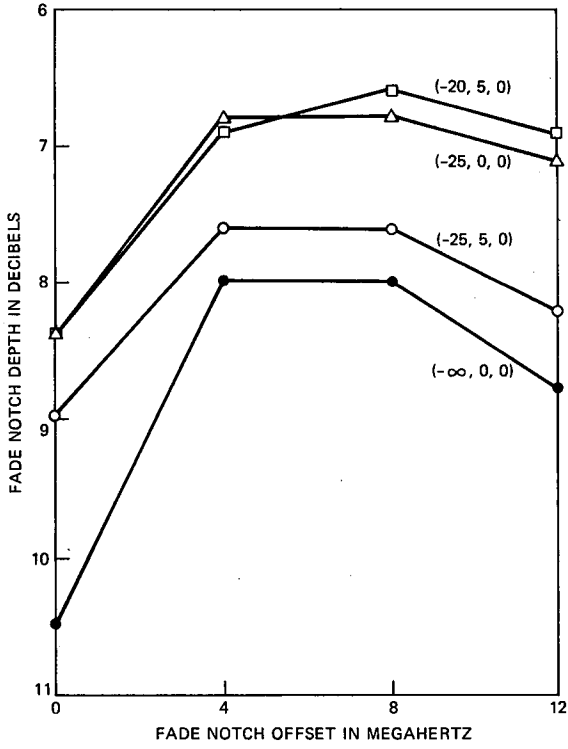

Fig. 9—Measured performance signatures for dual-polarized 16-QAM radio; $\Gamma = 0.45$, $T_s = 1/(22.5$ Mbaud), $s/n = 60$ dB.

The next phase of the experimental study was to increase the flat fade level from −25 to −20 dB and to introduce a notch-centered 5-dB fade, thus the triplet (−20, 5, 0). The resulting performance signature curve is also shown in Fig. 9 and supports the theoretical data of Fig. 4. In general, conclusions drawn from the experimental data support our theoretical findings. Note that in all of the experimental tests, the two transmitters were completely independent of one another; hence, the conditions $0 \leq \tau_m \leq T_s$ and $0 \leq \theta_m \leq 2\pi$ actually held.

VI. CONCLUSIONS

In this paper we present computed performance signatures for dual-polarized transmission of M-QAM signals over dispersive multipath digital radio channels. For the assumed model, we show that a cross-coupled interferer exhibits noiselike behavior, and its power loss, whether flat or midly dispersive, brings about an improvement (reduction) in dual-polarized system outage time. The theoretical findings

are supported by measured performance signatures obtained from a laboratory simulation of the analytic model.

REFERENCES

1. A. J. Giger and W. T. Barnett, "Effects of Multipath Propagation on Digital Radio," IEEE Trans. Commun., *COM-29*, No. 2 (December 1979), pp. 1870–5.
2. G. J. Foschini and J. Salz, "Digital Communications Over Fading Radio Channels," B.S.T.J., *62*, No. 2, Part I (February 1983), pp. 429–59.
3. H. Sari, "A Comparison of Equalization Techniques on 16-QAM Digital Radio Systems During Selective Fading," Globecom '82 Conf. Rec. (November–December 1982), pp. F3.5.1–6.
4. N. Amitay and L. J. Greenstein, "Multipath Outage Performance of Digital Radio Receivers Using Finite-Tap Adaptive Equalizers," IEEE Trans. Commun., *COM-32*, No. 5 (May 1984), pp. 597–608.
5. G. L. Fenderson et al., "Adaptive Equalization of Multipath Propagation for 16-QAM 90-Mb/s Digital Radio," AT&T Bell Lab. Tech. J., *63*, No. 8 (October 1984), pp. 1447–63.
6. C. A. Siller, Jr., "Multipath Propagation: Its Associated Countermeasures in Digital Microwave Radio," IEEE Commun. Mag., *22*, No. 2 (February 1984), pp. 6–15.
7. M. Kavehrad, "Performance of Cross-Polarized M-ary QAM Signals Over Nondispersive Fading Channels," AT&T Bell Lab. Tech. J., *63*, No. 3 (March 1984), pp. 499–521.
8. W. D. Rummler, "A New Selective Fading Model: Application to Propagation Data," B.S.T.J., *58*, No. 5 (May–June 1979), pp. 1037–71.
9. M. Emshwiller, "Characterization of the Performance of PSK Digital Radio Transmission in the Presence of Multipath Fading," ICC '78 (June 1978), pp. 47.3.1–6.
10. C. W. Lundgren and W. D. Rummler, "Digital Radio Outage Due to Selective Fading—Observation Versus Prediction From Laboratory Simulation," B.S.T.J., *5* (May–June 1979), pp. 1073–100.
11. R. W. Lucky, J. Salz, and E. J. Weldon, Jr., *Principles of Data Communications*, New York: McGraw-Hill, 1968.
12. P. E. Butzien, private communication.
13. M. Schwartz et al., *Communication Systems and Techniques*, New York: McGraw-Hill, 1966.
14. G. H. Golub, and J. H. Welsch, "Calculations of Gauss Quadrature Rules," Math. Comp., *26*, No. 106 (April 1969), pp. 221–30.
15. V. K. Prabhu, "Some Considerations of Error Bounds in Digital Systems," B.S.T.J., *50* (December 1971), pp. 3127–52.
16. J. J. Kenny, "Digital Radio for 90-Mb/s, 16-QAM Transmission at 6 and 11 GHz," Microw. J., *25*, No. 8 (August 1982), pp. 71–80.
17. M. Kavehrad, "Performance of Nondiversity Receivers for Spread Spectrum in Indoor Wireless Communications," AT&T Tech. J., *64*, No. 6 (July–August 1985), pp. 1181–210.

AUTHORS

Mohsen Kavehrad, B.S. (Electrical Engineering), 1973, Tehran Polytechnic Institute; M.S. (Electrical Engineering), 1975, Worcester Polytechnic Institute; Ph.D. (Electrical Engineering), 1977, Polytechnic Institute of New York; Fairchild Industries, 1977–1978; GTE, 1978–1981; AT&T Bell Laboratories, 1981—. At AT&T Bell Laboratories Mr. Kavehrad is a member of the Communications Methods Research Department at Crawford Hill Laboratory. His research interests are digital communications and computer networks. He has organized and chaired sessions for IEEE sponsored conferences. Technical Editor, IEEE Communications Magazine; Chairman, IEEE Communications Chapter of New Hampshire, 1984; Member, IEEE, Sigma Xi.

Curtis A. Siller, Jr., B.S.E.E., 1966, M.S. (Plasma Physics), 1967, Ph.D. (Electrical Engineering), 1969, The University of Tennessee at Knoxville;

AT&T Bell Laboratories, 1969–1978, 1979—. At AT&T Bell Laboratories, Mr. Siller has analyzed and designed reflector antennas for terrestrial microwave communications; performed exploratory investigations of digitally implemented adaptive transversal equalizers for high-speed digital radio systems; identified novel approaches to digital FIR filtering and quadrature amplitude modulation; and explored new algorithms for the stable control of fractionally spaced equalizers. Mr. Siller has authored nearly 30 papers in the aforementioned areas and is presently involved in system engineering of future digital transmission systems. He is the recipient of an AT&T Bell Laboratories Distinguished Technical Staff Award. Senior Member, IEEE, where he serves on the Signal Processing and Communication Electronics Technical Committee, and has helped plan the technical program for several international conferences; Member, Phi Eta Sigma, Eta Kappa Nu, Tau Beta Pi, Phi Kappa Phi, Sigma Xi, New York Academy of Sciences.